

NONLINEAR OPTICAL MATERIALS

1. Introduction

Nonlinear optical (NLO) materials are the building blocks of the emerging technologies of optoelectronics and photonics (the acquisition, transmission, processing, and storage of information using photons or light quanta). The interactions between photons are weak compared to interactions between electrons, thus long distance transmission of information over fiber optic lines (see FIBER OPTICS) with minimal signal degradation is facilitated. Moreover, compared to electronics, optoelectronics and photonics offer advantages in terms of speed (bandwidth) of information processing as high frequency signals are less degraded than with transport by electrons through metal wires.

Analogous to electronic materials, nonlinear optical materials can be divided into two classes: linear (passive) and nonlinear (active) (1–6). Linear materials are employed in the construction of transmission lines (waveguides), power and polarization splitters, gratings, etc; nonlinear materials are used in the construction of switches, modulators, frequency doublers and triplers, active beam steering elements, limiters, amplifiers, rectifiers, and transducers. Nonlinear optical phenomena arise when applied external fields, ie, either high frequency [visible or infrared (ir) wavelength light] or low frequency [dc electrical, radio frequency (rf), microwave, or millimeter wave] fields, are sufficiently strong to compete with internal electrostatic interactions. Thus, nonlinear optical materials are typically those containing weakly bound (highly polarizable) electrons. Nonlinear optical phenomena include harmonic generation, sum- and difference-frequency generation, optical parametric oscillation, rectification, intensity-dependent refraction, phase conjugation, multiple wave mixing, Raman scattering, Brillouin scattering, induced opacity and reflectivity, multiple photon absorption and emission, and electrooptic modulation.

Further subclassification of nonlinear optical materials can be explained by the following two equations of microscopic, ie, atomic or molecular, polarization, p , and macroscopic polarization, P , as power series in the applied electric field, E (disregarding quadrupolar terms):

$$p = \alpha E + \beta EE + \gamma EEE + \dots \quad (1)$$

where α is the linear polarizability, β and γ ; are the first and second (atomic or molecular) hyperpolarizabilities, respectively; and

$$P = \chi^{(1)}E + \chi^{(2)}EE + \chi^{(3)}EEE + \dots \quad (2)$$

where $\chi^{(1)}$ is the linear optical susceptibility, $\chi^{(2)}$ the second-order NLO susceptibility, and $\chi^{(3)}$ the third-order NLO susceptibility. The second-order coefficients are typically zero for centrosymmetric symmetries. Typical of power series expressions, the magnitudes of the coefficients decrease for higher order terms. Realized and known practical applications of third-order optical nonlinearity are rare and terms beyond third order can be ignored. The small magnitudes of optical nonlinearities often require long interaction lengths, eg, as found in

waveguides, for reasonable device performance. Each coefficient is complex with a real component corresponding to index of refraction phenomena and an imaginary component corresponding to absorption phenomena. Real and imaginary components are related by the Kramers-Kronig relationship (1,2). When speaking of NLO devices, it is common to speak of exploiting either a nonlinear index change only or a nonlinear absorption change only. Nonlinear index of refraction changes are typically exploited in regions of transparency, ie, regions far removed from one-photon resonances, but nonlinear absorption phenomena are usually exploited near resonance.

Materials are also classified according to a particular phenomenon being considered. Applications exploiting off-resonance optical nonlinearities include electrooptic modulation, frequency generation, optical parametric oscillation, and optical self-focusing. Applications exploiting resonant optical nonlinearities include sensor protection and optical limiting, optical memory applications, biomedical imaging, etc. Because different applications have different transparency requirements, distinction between resonant and off-resonance phenomena are thus application specific and somewhat arbitrary.

Nonlinear optical materials can also be classified according to atomic composition into organic and inorganic materials. Inorganic materials range from crystalline lithium niobate [12031-63-9], LiNbO_3 , to amorphous semiconductor materials such as gallium arsenide [1303-00-0], GaAs (see ELECTRONIC MATERIALS, SEMICONDUCTORS). Organic materials can be either crystalline such as polydiacetylene, or polymeric materials incorporating a variety of organic chromophores such as disperse red 1 [2872-52-8], 4-(*N*-ethyl-*N*-2-hydroxyethyl)amino-4'-nitroazobenzene. For most organic materials, however, the optical nonlinearity can be associated with weakly bound π -electrons. As of this writing (~late-2002), no single material has been proven suitable for extensive commercial applications, thus discussion herein focuses on the material requirements for various applications.

2. Second-Order Nonlinear Optical Materials

Classes of second-order material applications can be understood by noting the sinusoidal nature of electromagnetic radiation and rewriting equation 2 for the case of two different electromagnetic radiation fields (denoted i and j) interacting with a nonlinear optical material (equation 3a) or a single ($\omega_i = \omega_j$) high frequency field (equation 3b) interacting with a nonlinear optical material.

$$P = [\chi^{(1)} + \chi^{(2)} E_{0j} \cos(\omega_j t - k_j z)] E_{0i} \cos(\omega_i t - k_i z) + \dots \quad (3a)$$

$$P = \chi^{(1)} E_0 \cos(\omega t - kz) + (1/2)(E_0)^2 [1 + \cos(2\omega t - 2kz)] + \dots \quad (3b)$$

where ω is the frequency of the electromagnetic radiation, t the time, and k and z are the wave vector and spatial coordinate (position), respectively. The symbol “ i ” is used to denote an optical (visible or ir wavelength) electromagnetic

field while the symbol “ j ” typically denotes a low frequency (dc to terahertz) electromagnetic field.

Two obvious applications can be identified for second-order NLO materials: frequency doubling, ie, the 2ω term of equation 3b; and electrooptic modulation, ie, the second term in brackets of equation 3a. Frequency doubling results in the generation of a new light beam at twice the frequency (or one-half the wavelength) of the original light beam. For example, the generation of light at 532-nm wavelength can be realized by doubling the 1064-nm light from a yttrium aluminum garnet (YAG) laser (see LASERS). The low frequency term is associated with electrooptic (EO) modulation, ie, the Pockel’s effect and can be characterized by frequencies ranging from 0 Hz (dc) to 10 THz; that is, frequencies that span the radio frequency, microwave, millimeter, and submillimeter wave regions.

The fundamental phenomenon of Pockel’s effect is a phase change, $\Delta\phi$, of a light beam in response to a low frequency electric field of voltage, V . Relevant relationships for colinear electrical and optical field propagation are as follows (1–10):

$$\Delta\phi = \pi n^3 r_{\text{eff}} V L / \lambda h, \quad r_{\text{eff}} = -8\pi\chi^{(2)} / n^4 \quad \text{and} \quad V_{\pi} L = \lambda h / n^3 r_{\text{eff}} \quad (4)$$

where n is the index of refraction, r_{eff} the effective electrooptic coefficient, L the modulation length, h the gap distance between the electrodes (sample thickness), λ ; the optical wavelength, and V_{π} the voltage required to realize a phase shift of π . Sometimes a parameter Γ is added to the denominator of the $V_{\pi} L$ equation to take into account the radiofrequency field coupling efficiency, ie, losses owing to the resistivity of metal drive electrodes and incomplete mode overlap of optical and radiofrequency waves. Consequently, the $V_{\pi} L$ product is a measure of the modulation efficiency of the device. The Pockel’s effect is used to transduce electrical signals into optical signals, as, eg, in the cable television industry, for photonic detection of radar, for voltage sensing in the electric power industry, and to effect switching in local area networks. A variety of specialized applications such as phased array radar, optical gyroscopes, electromagnetic signal generation, active wavelength division multiplexing, etc, also exist. The most commonly encountered device configurations are shown in Figure 1. For the Mach-Zehnder configuration, the phase shift induced in one branch of the modulator by Pockel’s effect results in amplitude modulation when the modulated and unmodulated beams are recombined at the output.

$$I_o = I_i \sin^2[(\phi_{ba} + \Delta\phi)/2] \quad \text{and} \quad (V_{\pi} L)_{\text{MZ}} = \lambda h / n^3 r_{33} \quad (5)$$

where I_i and I_o are, respectively, the input and output intensities, ϕ_{ba} is the phase difference between the two arms, $\Delta\phi$ is the phase modulation produced by the EO effect, and the subscript MZ denotes Mach-Zehnder.

The birefringent (BR) modulator makes use of polarized light and tensorial nature of the electrooptic coefficient. For example, poled organic polymer films are characterized by two nonzero components for the electrooptic tensor: r_{33} and r_{13} , parallel and orthogonal to the poling direction, respectively. In order to obtain amplitude (intensity) modulation, the input beam is 45° polarized to

excite both transverse electric (TE) and transverse magnetic (TM) modes. An analyzer then converts the polarization modulation into an amplitude modulation:

$$\Delta n(\text{TE}) = n^3 r_{13} V / 2h \quad \Delta n(\text{TM}) = n^3 r_{33} V / 2h \quad (6)$$

$$\Delta \phi(\text{TE/TM})_{\text{sp}} = 2\pi \Delta n L / \lambda = \pi V L (n^3 r_{13} - n^3 r_{33}) / \lambda h \quad (7)$$

$$I_o = I_i \sin^2[(\phi_{\text{sp}} + \Delta \phi_{\text{sp}}) / 2] \quad (V \pi L)_{\text{BR}} = 1.5 (V \pi L)_{\text{MZ}} \quad (8)$$

Compared to the Mach-Zehnder modulator, the modulation efficiency of the birefringent modulator is lower because $V_\pi L$ is 1.5 times higher, ie, $r_{33} = 3r_{13}$ for dipolar chromophores. Directional couplers (Fig. 1c) consist of two side-by-side waveguides separated by a few micrometers. The overlap of the guided waves in the two waveguides couples energy back and forth between the waveguides. When a low frequency voltage is applied, the intensities at the output ports are determined by either modulation of the phase mismatch, $\Delta \phi$, or the coupling coefficient, $\Delta \beta$. The smallest voltage required for switching is 1.7 times larger than that of a Mach-Zehnder device.

Two parameters that characterize the performance of electrooptic modulators are $V_\pi L$ and the length–bandwidth product given by the following:

$$L \Delta \omega = c / 4 \left[n(\omega) - \epsilon_{\text{eff}}^{1/2} \right] \quad (9)$$

where ϵ_{eff} is the dielectric constant. The length–bandwidth product is defined by the velocity mismatch of the optical and the low frequency/long wavelength (radio, micro, or millimeter) waves propagating in the material. In Table 1, drive voltage and bandwidth characteristics for three of the most promising and diverse classes of electrooptic materials are compared. Although single-crystal lithium niobate permits realization of digital-level drive voltages, the bandwidth is limited to tens of gigahertz unless sophisticated device architectures are employed, which in turn require higher drive voltages. Lithium niobate also exhibits a relatively low (0.1 GW/cm^2) optical damage threshold owing to its large photorefractive effect.

For organic EO materials such as polymers, both n and ϵ are determined by the π -electrons of the NLO chromophore and $n^2 \approx \epsilon$ leading to bandwidths $\gg 100 \text{ GHz}$ for a 1-cm device length. Operation of organic polymer Mach-Zehnder electrooptic modulators has been demonstrated for frequencies as high as 1.6 THz (8,11) with 3dB bandwidths demonstrated to 200 GHz . Unlike crystalline inorganic NLO materials, organic chromophores seldom assemble naturally in noncentrosymmetric space groups. Moreover, when organic NLO crystals are obtained, these are usually characterized by growth anisotropy that renders the crystals unusable for device applications. To obtain noncentrosymmetric macroscopic lattices of organic NLO chromophores, extensive use has been made of sequential synthesis and electric field poling methods.

Sequential synthesis film fabrication approaches include Langmuir-Blodgett methods, Merrifield-type covalent coupling reactions, sequential synthesis

exploiting ionic interactions, and molecular beam epitaxy methods (5,7,8,12). Unfortunately, to prepare films on the order of 1 μm , required for device fabrication, a high degree of perfection is required for the deposition of each layer. As of this writing (late-2002), sequential syntheses are still not competitive for the fabrication of electrooptic modulators, even though these methods are of great interest for frequency doubling applications because of opportunities afforded for phase-matched second harmonic generation (see THIN FILMS, FILM FORMATION TECHNIQUES). However, the research of Tobin Marks and co-workers (13) on Merrifield-type sequential synthesis is making dramatic progress and may lead to practical devices over the next few years; this research certainly merits watching.

The method of choice for the fabrication prototype devices using organic EO materials appears to be the electric field poling of NLO chromophores in polymer matrices near the glass-transition temperature, T_g , of the polymer matrix. A deficiency of this approach is the relaxation of poling-induced order when the poling field is removed. To overcome this problem, a variety of lattice-hardening reactions have been developed. These have generally been successful in permitting the fabrication of NLO-active polymer lattices that can withstand temperatures on the order of 100°C for long (thousands of hours) periods of time and even higher temperatures for such short periods of time as associated with the deposition of metal electrodes (5,7,8,12). The final glass-transition temperature appears to be the critical parameter in defining the long-term stability of poling-induced optical nonlinearity both for chromophore–polymer composites and for chromophores covalently attached to the polymer host lattices (5,7,8,12). Certain advantages have also been observed for the covalent incorporation of chromophores relative to chromophore–polymer composites. These include the realization of higher chromophore number densities, prevention of phase separation and chromophore aggregation, avoidance of chromophore sublimation at high processing temperatures, reduced plastization of the polymer lattices for a finite chromophore loading, elimination of poling-induced light scattering arising from an inhomogeneous distribution of chromophores, and avoidance of chromophore extraction with application of cladding layers in the fabrication of EO modulator waveguide structures (see COMPOSITE MATERIALS, THERMOPLASTIC POLYMER-MATRIX). Recently, improvement in the performance of organic electrooptic materials has been realized by incorporation of chromophores into dendritic supramolecular architectures (14). Such materials have lead to improved electrooptic activity, reduced optical loss, and improved stability of electrooptic activity (8,14).

A putative advantage of organic NLO materials over crystalline inorganic materials is that active chromophores can be systematically varied in the former to increase optical nonlinearity (Table 2) (15–22). The large hyperpolarizabilities realized since 1999 have permitted the fabrication of prototype Mach Zehnder devices operating with drive voltage requirements of less than one volt (23). An even more important feature of polymeric materials is that they can be readily integrated with semiconductor electronics and fiber optic transmission lines. Buried channel nonlinear optical waveguides can be fabricated by a variety of techniques, including reactive ion etching and electron cyclotron resonance etching, photochemical lithography, and spatially selective poling (8,24,25). Mechanically stable coupling to silica fibers can be accomplished by silicon

V-groove techniques (8). As the name implies, silicon V-groove technology involves etching a V-shaped groove in a silicon substrate, positioning a silica fiber in that groove against the electrooptic waveguide, and overcoating the fiber with electrooptic polymer.

Second-order nonlinear optical organic chromophores have also been incorporated into inorganic lattices such as SiO_2 by sol-gel techniques (26). Such lattices hold the potential for reduced optical loss due to low proton content and for good thermal stability because of extensive three-dimensional cross-linking.

The inorganic material lithium niobate exists as single crystals and cannot be readily grown on other substrates. There have, however, been attempts at growth on semiconductor substrates. Channel waveguides have been obtained through ion or proton exchange involving lithium niobate single crystals, and lithium niobate films have been grown heteroepitaxially on lithium tantalate, LiTaO_3 , single crystalline substrates (27). Because of the difficulty entailed in obtaining lithium niobate waveguides on semiconductor substrates, lithium niobate modulators are typically flip-chip bonded to a substrate; or alternatively, the electronics, fibers, and modulators are interconnected via cables and fibers (28). An effort has also been made to obtain all-semiconductor systems that rely primarily on GaAs or related compounds for both optical and electronic components (see PACKAGING, ELECTRONIC MATERIALS) (29).

The market for electrooptic modulators is uncertain at this time; much of the motivation for developing prototype devices derives from anticipated needs of the telecommunications, computing, and defense industries. Various corporate research laboratories have produced prototype modulators that can operate to 60 GHz (8,30–39) or even higher (11). Nontechnical issues such as the early implementation of direct (satellite transmission) television and the development of improved modulated lasers may also affect the long term market success of electrooptic modulators.

Second-order NLO materials can be used to generate new frequencies through second harmonic generation (SHG), sum and difference frequency mixing, and optical parametric oscillation (OPO). The first, SHG, is given in equation 3b.

Second harmonic generation has some of the same material requirements as electrooptic modulation; for instance, a significant magnitude of $\chi^{(2)}$ that translates by a linear relationship into an adequate SHG coefficient, d . However, compared to electrooptic modulation, SHG has a more stringent transparency requirement because transparency is needed at both the fundamental and the second harmonic wavelengths. A more challenging requirement for SHG is to avoid destructive interference by phase matching the fundamental and second harmonic. For a colinear propagation of the fundamental and second harmonic beams, the wave vector difference between the two waves is given by the following, where $k = n\omega/c$:

$$\Delta k = k_{2\omega} - 2k_{\omega} \quad (10)$$

This equation leads to a variation of the second harmonic power, given by

$$P(2\omega) = \left\{ 128\pi^5 [P(\omega)]^2 / WN(2\omega)_{\text{eff}} N^2(\omega)_{\text{eff}} \lambda^2 c \right\} \cdot (F_{112})^2 \int |\chi^{(2)}(x) \exp(i\Delta kx) dx|^2 \quad (11)$$

where N is the mode index, W the spatial extent of the fundamental in the y direction, and F_{112} the normalized overlap integral. If a periodic variation of $\chi^{(2)}$ exists along x such that

$$\chi^{(2)}(x) = \chi^{(2)}(a) + \chi^{(2)}(b) \cos(2\pi x/\Lambda) \quad (12)$$

where Λ is the grating period, then the integral of equation 11 has a nonvanishing value of $\chi^{(2)}(b)/2$. This method of phase matching is called quasi phase matching (5,10,40) and has been applied to both inorganic and organic materials. For example, quasi-phase-matched SHG has been observed for LiNbO_3 , LiTaO_3 , potassium titanyl phosphate (KTP) [109657-81-0], KTiOPO_4 , crystals as well as for NLO chromophore-containing polymers. The required periodic domain structures were obtained by proton exchange (41,42), titanium diffusion (43,44), asymmetric temperature growth (45), laser-heat pedestal growth (46,47), quick heat treatment (48), electron injection (49), and electric field poling (50). Quasi phase matching in organic polymeric thin films has been accomplished by photochemical processing (51) and electric field poling (52).

Phase matching in crystalline materials is typically achieved by using birefringence associated with different propagations to offset the natural dispersion in the medium (5,10). This can be accomplished either through angle or by temperature tuning. Other methods of achieving phase matching of the fundamental and second harmonic waves copropagating in the material include the use of anomalous dispersion, Cerenkov radiation, and counterdirected waves (5,10). A variety of material processing schemes have been utilized to achieve the particular geometries required for many phase-matching schemes.

As with electrooptic materials, materials for frequency doubling can also be divided into first generation inorganic crystalline materials and second generation organic materials. Such division, however, does not imply that inorganic materials are obsolete. Indeed, only inorganic materials have achieved commercial success as frequency doublers for ir lasers. Representative inorganic materials are listed in Table 3 (5,10). Owing to the relatively low nonlinear coefficients, d , of most inorganic materials, long interaction lengths are usually required; these, in turn, necessitate large, high quality single crystals. Efforts have also been made to fabricate nonlinear optical waveguides. Single-crystal films are often used to avoid light scattering problems. For organic materials, the trade-off between optical nonlinearity and optical transparency continues to be a problem. Materials having large d (eg, 50–400 pm/V) values typically exhibit finite absorption at the second harmonic. This is especially problematic in attempting to develop frequency doublers for diode lasers operating at ~ 820 nm. Research, however, has focused on extending the window of transparency of organic frequency doubling materials into the blue (53,54). A commonly quoted (10) figure of merit (FOM) for frequency doubling materials is d^2/n^3 , where d is the second

harmonic generation coefficient and n the index of refraction. If this relationship is applied to the materials in Table 1, a value of ~ 4 is obtained for lithium niobate and a value of ~ 500 or greater for NLO polymers. Obviously, such a FOM is useful only if the materials in question can satisfy the transparency requirements of a particular application.

Commercial frequency doublers have relied on inorganic materials. The commercial future of doublers depends on not only the improvement in second-order materials but also the development of diode lasers capable of operating in the visible frequency domain.

The need for frequency-agile laser sources has driven the development of optical parametric oscillators (OPOs) and optical parametric amplifiers (OPAs). A variety of these devices have become available from commercial laser component suppliers such as Continuum and Spectra Physics. Both OPOs and OPAs rely on difference frequency generation. For operation in the visible frequency domain, inorganic materials such as β -barium borate [13701-59-2], BaB_2O_4 , or KTP are required (55). Because organic chromophores have band edges that extend through much of the visible spectral region, use is limited to the near infrared (56). Both OPOs and OPAs have been developed for use with femtosecond pulses as well as longer pulses and the operation of laser systems using these components has been greatly simplified. The OPO and OPA technology has had a dramatic effect on promoting the utilization of frequency agile pulsed laser systems.

In a spatial light modulator, light impinges on a photoconductor, eg, amorphous silicon, that is reverse-biased with an applied voltage. Charge carriers are formed in the photoreceptor in an imagewise fashion. The pattern of charge then drifts, under the influence of the field, to the interface between the light blocking layer and the photoreceptor where it is trapped. Electric field gradients are generated in an adjacent electrooptic film which, in turn, generates patternwise variations in the electric field-dependent refractive index in the electrooptic layer. A readout beam, impinging on the electrooptic film side of the modulator, is then used to decipher the information stored in the electrooptic film. The electrooptic layer can be either a liquid crystalline material or a second-order NLO material (Pockel's effect). Several types of electrooptic materials have been utilized in the construction of spatial light modulators; eg, potassium dihydrogen phosphate has been used in conjunction with high resistivity silicon to construct a device having spatial resolution approaching 10 line pairs/mm and frame-grabbing rates of 1 kHz (57). Although second-order nonlinear optical materials permit high data rates, their small electrooptic coefficients do not permit them to compete effectively with liquid crystalline materials (qv).

Recently, organic electrooptic materials have been employed for laser beam steering using a cascaded prism arrangement to increase the effective interaction length (58–60). Such devices permit realization of dramatically faster beam steering speeds; however, further reduction of drive voltage requirements will be necessary for practical applications.

Recently, organic electrooptic materials have been incorporated into ring microresonator structures (61,62). The coupling of light into such structures is predicated on satisfying two conditions; namely, that the circumference of the ring be a multiple of the wavelength of light and that the velocity of light in

the ring match the input velocity (ie, that the index of refraction in the ring and input waveguides be the same). A ring resonator fabricated from an electrooptic material permits voltage-controlled coupling of light into a ring microresonator. Thus, such a device can act as a wavelength selective filter. Since electric signals can be transduced onto an optical carrier in an electrooptic ring waveguide such structures can also be used to construct active wavelength division multiplexing (WDM) transmitter/receiver systems. In studies of prototype devices, Rabiei and co-workers (61,62) demonstrate wavelength selectivity of 0.01 nm and per channel bandwidths of 15 GHz for active WDM devices fabricated from organic electro-optic materials. A figure of merit of 2 GHz/V was demonstrated in these initial studies. More recently, these workers have demonstrated double as well as single ring resonator devices. Such structures were employed to demonstrate laser tuning across the 1.55- μ telecommunications band. Signal processing of both digital and analog data has been demonstrated at both 1.3 and 1.55- μ telecommunication bands.

Another area of research activity related to second order nonlinear optical material worthy of noting is the study of octupolar materials by Zyss and co-workers (63–67). While these materials have yet to be used for device prototyping, optical nonlinearities have been improved significantly in the past several years.

An area of second-order nonlinear optical materials receiving increased attention is terahertz signal generation and detection; however, this must be viewed as a basic research effort at this point in time.

3. Third-Order Nonlinear Optical Materials

Third-order processes include third harmonic generation (THG), self-focusing, self-defocusing, self-phase modulation, saturable absorption, and reverse saturable absorption. Because of the weak magnitude of third-order optical nonlinearities, known practical applications are rare; the few applications that do exist typically exploit long interaction lengths. A wide range of materials have been studied in the search for materials containing usable optical nonlinearities; such materials include inorganic crystals and glasses; doped glasses; simple gases and liquids (atomic and molecular as well as organic and inorganic); semiconductors; quantum dots, wells and wires; conductive particle composites; organic and polymer crystals; amorphous organic and inorganic polymers; and biological complexes. Mechanisms of optical nonlinearity can be found in the literature for many types of optical nonlinearity and various classes of materials contributing to these nonlinear phenomena.

The index of refraction, n , can be expressed for nonlinear optical materials as

$$n = n_0 + n_2 I \quad (13)$$

where I is the intensity of light and n_2 , the nonlinear index, can be related to the third-order susceptibility by

$$n_2 = 16\pi^2 \chi^{(3)} / c(n_0)^2 \quad (14)$$

where n_0 is the linear index of refraction and c is the speed of light. Index of refraction phenomena are typically associated with the bending of a light beam or a phase shift of light passing through a material.

Nonlinear refraction phenomena, involving high intensity femtosecond pulses of light traveling in a rod of Ti:sapphire, represent one of the most important commercial exploitations of third-order optical nonlinearity. This is the realization of mode-locking in femtosecond Ti:sapphire lasers (qv). High intensity femtosecond pulses are focused on an output port by the third-order Kerr effect while the lower intensity continuous wave (CW) beam remains unfocused and thus is not effectively coupled out of the laser.

The dynamic Kerr effect (DKE) is the third-order analogue of the second-order Pockel's effect. DKE also gives rise to phase shifts given by

$$\Delta\phi = 2\pi\Delta nFL/\lambda \quad (15)$$

where $\Delta n = n_2 I$ and F accounts for any cavity resonance enhancement. However, in the Kerr effect, the field controlling the nonlinear phase shift is an optical field leading to an all-optical control of phenomena such as local area network switching. Indeed, prototype devices have been produced that are competitive in performance with electrooptic switches.

A crucial advantage of switching exploiting the DKE over switching based on the Pockel's effect is that the switching speed for the latter is limited at high speeds by electrode resistivity (11). In contrast, switching exploiting the DKE is typically limited by phase relaxation times that are on the order of a few hundred femtoseconds. The disadvantage of DKE switches, however, is the long interaction length required. The dynamic Kerr effect has been utilized in nonlinear optical loop mirrors (NOLMs) and tetrahertz optical asymmetric demultiplexers (TOADs) to produce ultrafast (eg, 100 Gbits/s) all-optical demultiplexing. Both silica fiber and semiconductor materials have been used in device performance demonstrations (68–71).

In an effort to identify materials appropriate for the application of third-order optical nonlinearity, several figures of merit (FOM) have been defined (1–6,9,10,72–74). Parallel all-optical (Kerr effect) switching and processing involve the focusing of many images onto a nonlinear slab where the transmissive characteristics are a function of the total light intensity. The interaction length and focal spot size are limited by diffraction. For a phase shift greater than π to be achieved, n_2 must be $> n_0 \lambda^2 / (4FP_s)$, where P_s is the laser power. For $P_s = 10$ mW, $F = 1$, and $\lambda = 1 \mu\text{m}$, n_2 must then be $> 10^{-11} \text{ m}^2/\text{W}$. This requires $\chi^{(3)}$ to be $> 10^{-5}$ esu, which is a number very difficult to achieve. Because in serial configurations light is confined in a waveguide, a smaller optical nonlinearity can be compensated for by a longer interaction length. The practical interaction length, L , is limited by optical losses; it is described by $L = A/\alpha$, where A is the acceptable loss and α the attenuation coefficient. The optically induced phase shift is then given by

$$\Delta\phi = 2\pi\Delta nFA/\lambda\alpha \quad (16)$$

Both nonlinear and linear absorption can contribute to losses (10,74), ie,

$$\alpha = \alpha_1 + \alpha_2 I + \alpha_3 I^2 + \dots \quad (17)$$

where α_1 , α_2 , and α_3 are the one photon (linear) absorption, two-photon (non-linear) absorption, and three-photon (nonlinear) absorption coefficients, respectively. One FOM definition for serial processing is

$$W = n_2 I / \lambda \alpha_1 \quad (18)$$

for one-photon absorption, and

$$T^{-1} = n_2 / 2\lambda \alpha_2 \quad (19)$$

for two-photon absorption. The switching power of channeled devices can be estimated from

$$P_s = \Delta\phi / (n_2 L / \sigma_{\text{eff}}) \quad (20)$$

where σ_{eff} is the effective waveguide cross-sectional area.

Besides W , there are two other definitions of FOM for all-optical processing:

$$W' = n_2 / \alpha \quad \text{and} \quad W'' = n_2 / \alpha \tau \quad (21)$$

where τ is the switching speed. Any nonlinearity, even a thermal effect, can turn on instantaneously. In order to avoid cross-talk for series pulses, the relaxation time of the optical nonlinearity, τ , must be short. The first definition (W) emphasizes the maximum nonlinear phase shift obtainable in conjunction with the lowest loss. The second definition (W') focuses on the trade-off between nonlinear response and optical loss. The third definition (W'') also takes relaxation time into account. Comparing materials using these different definitions is important because FOMs always vary with offset from one- and two-photon resonances. A rough comparison of four examples representing four classes of materials is presented in Table 4. To provide the most meaningful comparison, optical nonlinearities have been measured far from resonance. High FOM for silica glasses is not particularly meaningful because unrealistically long interaction lengths would be required. It is usually impractical to build devices limited by such space requirements.

For measurements carried out closer to resonances, thermal contributions to the optical nonlinearity, given by the following formula, can compete with electronic contributions (75,76):

$$n_2(\text{thermal}) = (\alpha \tau_t / \rho C_p) (dn/dT) \quad (22)$$

where dn/dT is the thermo-optic coefficient, ρ the density of the material, C_p the specific heat capacity at constant pressure, and τ_t the thermal relaxation time.

Degenerate four-wave mixing (DFWM) is also called phase conjugation or real-time holography (qv). It is a Kerr-type phenomenon where irradiation of a sample using three beams results in a fourth beam that satisfies wave vector conservation. In other words, two beams are used to write a grating that is read by a third beam, which generate a signal that is the phase conjugate to the reading beam. DFWM can be employed as an optical signal processing technique. When an object beam is scrambled by propagating through an aberrating medium, the conjugate beam propagates back through the medium along the same path as followed by the object wave. The scrambling is thus undone. Such devices are useful when high power laser beams must be brought into tight focus, or transmitted through the atmosphere, or used to produce a pattern.

Saturable absorption (hole-burning) is a change (typically a decrease) in absorption coefficient which is proportional to pump intensity. For a simple two level system, this can be expressed as

$$\alpha(I) = \alpha_0 / (1 + I/I_s) \quad (23)$$

where I_s , the saturation light intensity is equal to $\Delta E / (\sigma \cdot \tau)$, in which ΔE is the energy difference between the ground and excited state, σ the absorption cross-section, and τ the excited state to ground state relaxation time. One application of saturable absorption is in volatile computer memory, dynamic random access memory (DRAM), where the refresh time depends on excited state relaxation time. A tunable laser is used to write many spectral Bennett holes, ie, bits of information, within an inhomogeneously broadened spectrum at the same spatial location. The storage density, which can reach 10^7 , is given by the ratio of the inhomogeneous line width to the homogeneous packet width (77). Such a density is literally more than a thousand times better than the best video disk.

Reverse saturable absorption is an increase in the absorption coefficient of a material that is proportional to pump intensity. This phenomenon typically involves the population of a strongly absorbing excited state and is the basis of optical limiters or sensor protection elements. A variety of electronic and molecular reorientation processes can give rise to reverse saturable absorption; many materials exhibit this phenomenon, including fullerenes, phthalocyanine compounds (qv), and organometallic complexes.

An area of research on third order nonlinear optical materials to watch is that of developing materials with improved two photon absorption and luminescence (78,79). These materials can be used for a wide range of applications extending from three-dimensional photolithography to biomedical imaging.

4. Photorefractive Materials

Photorefractivity can be thought of as a four part process. Initially, pairs of spatial frequency modes of a single input beam interfere with the photorefractive material to produce a periodic intensity distribution. The input light causes impurities (inorganics) or electron donors/acceptors (organics) to release charges

(electrons or holes) that migrate through the dark regions of the material and become trapped. This results in a periodic charge distribution in the material which, in turn, yields a periodic electrical field. If no external electric field is present, this periodic electrical field is phase shifted by $\pi/2$ from the original light interference pattern. Finally, the induced space-charge field alters the refractive index periodically through the linear electrooptic effect. The index of refraction grating created in this manner combines with the intensities of the spatial frequency modes and introduces a nonlinear phase for each mode. The overall effect is a Kerr-like phenomenon realized with a second-order nonlinear optical chromophore. Photorefractive materials range from crystalline inorganic materials such as lithium niobate to organic polymer composites and homopolymer materials.

5. Economic Aspects

At the beginning of the twenty-first century, large-scale commercial applications have yet to be found for nonlinear optical materials. This situation could dramatically change over the next two decades. Among the most promising classes of materials for extensive commercial application are second-order materials for applications in the defense, computing, and telecommunications industries. Such applications include phased array radar, optical gyroscopes, chip scale wavelength division multiplexing, analogue-to-digital conversion, electrical-to-optic signal transduction (rf photonics), switching in optical networks, spatial light modulation and laser beam steering, high bandwidth signal generation, and sensing. A number of commercial suppliers of lithium niobate devices exists, such as United Technologies. Two companies (Lumera Corporation in Bothell, Wash. and Pacific Wave Industries in Los Angeles, Calif.) offer organic electrooptic modulators for sale. A small market also exists for frequency doublers based on inorganic crystalline materials. Similarly, a niche market application has been found for BBO and KTP materials for optical parametric oscillators and amplifiers. These devices are available through laser suppliers such as Coherent, Continuum, and Spectra Physics, commercial applications of third-order materials are even less common than they are for second-order materials. The most significant application is probably the exploitation of the dynamic Kerr effect to achieve mode locking in Ti:sapphire lasers.

BIBLIOGRAPHY

"Nonlinear Optical Materials" in *ECT* 4th ed., Vol. 17, pp. 287–302, by Larry R. Dalton, University of California; "Nonlinear Optical Materials" in *ECT* (online), posting date: December 4, 2000, by Larry R. Dalton, University of California.

CITED PUBLICATIONS

1. P. N. Prasad and D. J. Williams, *Introduction to Nonlinear Optical Effects in Molecules and Polymers*, Wiley-Interscience, New York, 1990.
2. R. W. Boyd, *Nonlinear Optics*, Academic Press, New York, 1992.
3. L. A. Hornak, *Polymers for Lightwave and Integrated Optics*, Marcel Dekker, New York, 1992.
4. H. S. Nalwa and S. Miyata, *Nonlinear Optics of Organic Molecules and Polymers*, CRC Press, Boca Raton, Fla., 1997.
5. L. R. Dalton and co-workers, *Molecular Electronics and Molecular Electronic Devices*, CRC Press, Inc., Boca Raton, Fla., 1993, pp. 125–207.
6. D. L. Wise and co-workers, *Electrical and Optical Polymer Systems: Fundamentals, Methods, and Applications*, World Scientific, Singapore, 1998.
7. L. R. Dalton and co-workers, *Ind. Eng. Chem. Res.* **38**, 8 (1999).
8. L. R. Dalton, *Advances in Polymer Science*, Vol. 158, John Wiley & Sons, Inc., New York, 2001, pp. 1–86.
9. J. F. Reintjes, *Encyclopedia of Modern Physics*, Academic Press, New York, 1990, pp. 361–414.
10. G. I. Stegeman and W. Torruellas, *Electrical, Optical, and Magnetic Properties of Organic Solid State Materials*, Materials Research Society, Pittsburgh, 1994, pp. 397–412.
11. M. Lee and co-workers, *Science* **298**, 1404 (2002).
12. L. R. Dalton and co-workers, *Adv. Mat.* **7**, 519 (1995).
13. Y. G. Zhao and co-workers, *Appl. Phys. Lett.* **79**, 587 (2001).
14. H. Ma and co-workers, *J. Am. Chem. Soc.* **123**, 986 (2001).
15. D. M. Burland, R. D. Miller, and C. A. Walsh, *Chem. Rev.* **94**, 31 (1994).
16. H. E. Katz and co-workers, *J. Am. Chem. Soc.* **109**, 6561 (1987).
17. L.-T. Cheng, *J. Phys. Chem.* **95**, 10643 (1991).
18. V. P. Rao and co-workers, *Proc. SPIE* **1775**, 32 (1992).
19. S. R. Marder and co-workers, *Science* **263**, 511 (1994).
20. C. W. Dirk, *Chem. Mater.* **2**, 700 (1990).
21. A. K. Jen and co-workers, *Mat. Res. Soc. Symp. Proc.* **328**, 413 (1994).
22. J. Woodford and co-workers, *J. Appl. Phys.* **89**, 4209 (2001).
23. Y. Shi and co-workers, *Science* **288**, 119 (2000).
24. S. Garner and co-workers, *IEEE J. Quant. Electron.* **35**, 1146 (1999).
25. A. Chen and co-workers, *Opt. Eng.* **39**, 1507 (2000).
26. F. Chaumel, H. Jiang, and A. Kakkar, *Chem. Mater.* **13**, 3389 (2001).
27. A. Baudrant, H. Vial, and J. Duval, *J. Cryst. Growth* **43**, 197 (1978).
28. C. Burke and co-workers, *J. Lightwave Tech.* **10**, 610 (1992).
29. L. Eldada and co-workers, *J. Lightwave Tech.* **10**, 1610 (1992).
30. D. Garton and co-workers, *Appl. Phys. Lett.* **58**, 1730 (1991).
31. C. C. Teng, *Appl. Phys. Lett.* **58**, 1538 (1992).
32. W. H. G. Horthuis and co-workers, *Proc. SPIE* **2025**, 516 (1993).
33. G. R. Mohlmann and co-workers, *Proc. SPIE* **2285**, 355 (1994).
34. A. J. Ticknor, G. F. Lipscomb, and R. Lytel, *Proc. SPIE* **2285**, 386 (1994).
35. B. A. Smith and co-workers, *Proc. SPIE* **2025**, 499 (1993).
36. J. I. Thackara and co-workers, *Proc. SPIE* **2025**, 564 (1993).
37. J. C. Chon and co-workers, *Proc. SPIE* **2285**, 340 (1994).
38. K. W. Beeson and co-workers, *Proc. SPIE* **2025**, 488 (1993).
39. J. C. Dubois, P. Robin, and V. Dentan, *Proc. SPIE* **2025**, 467 (1993).
40. J. A. Armstrong and co-workers, *Phys. Rev.* **127**, 1918 (1962).

41. K. Shinozaki and co-workers, *Appl. Phys. Lett.* **59**, 510 (1991).
42. K. Mizuuchi, K. Yamamoto, and T. Taniuchi, *Appl. Phys. Lett.* **59**, 1538 (1991).
43. K. Shinozaki and co-workers, *Appl. Phys. Lett.* **58**, 1934 (1991).
44. X. Cao, R. Strivastava, and R. V. Ramaswamy, *Opt. Lett.* **17**, 592 (1992).
45. Y. Lin, L. Mao, and S. Cheng, *Appl. Phys. Lett.* **59**, 516 (1991).
46. E. J. Lim and co-workers, *Appl. Phys. Lett.* **59**, 2207 (1991).
47. D. H. Jundt and co-workers, *Appl. Phys. Lett.* **59**, 2657 (1991).
48. K. Mizuuchi and K. Yomamoto, *Appl. Phys. Lett.* **60**, 1283 (1992).
49. W. Hsu and M. C. Gupta, *Appl. Phys. Lett.* **60**, 1 (1992).
50. F. Ahmed, *J. Bangladesh Acad. Sci.* **13**, 175 (1989).
51. L. R. Dalton and co-workers, in P. N. Prasad, ed., *Frontiers of Polymer Research*, Plenum Press, New York, 1992, pp. 115–123.
52. R. A. Norwood and G. Khanarian, *Electron. Lett.* **26**, 2105 (1990).
53. G. H. Cross and co-workers, *Proc. SPIE* **2285**, 11 (1994).
54. D. Hissink and co-workers, *Proc. SPIE* **2025**, 37 (1993).
55. *J. Opt. Soc. Am. B* **10**(9), **10**(11) (1993).
56. D. Josse and co-workers, **64**, 3655 (1994).
57. D. Armitage, W. W. Anderson, and T. J. Karr, *IEEE J. Quant. Elec.* **QE21**, 1241 (1985).
58. L. Sun and co-workers, *Proc. SPIE* 3950, **98** (2000).
59. L. Sun and co-workers, *Opt. Eng.* **40**, 1217 (2001).
60. J. H. Kim and co-workers, *Proc. SPIE* 4279, **37** (2001).
61. P. Rabiei and co-workers, *J. Lightwave Tech.* **20**, 1968 (2002).
62. P. Rabiei and co-workers, *Int. Opt. Commun.* **1**, 14 (2002).
63. J. Zyss and I. Ledoux, *Chem. Rev.* **94**, 77 (1994).
64. C. Andraud and co-workers, *Chem. Phys.* **245**, 243 (1999).
65. C. Minhaeng and co-workers, *J. Chem. Phys.* **116**, 9165 (2002).
66. H. LeBozec and co-workers, *Synth. Met.* **124**, 185 (2001).
67. Y. Xue-Lin and co-workers, *Proc. SPIE* **4106**, 222 (2000).
68. D. M. Patrick and A. D. Ellis, *Electron. Lett.* **29**, 227 (1993).
69. D. M. Patrick, A. D. Ellis, and D. M. Spirit, *Electron. Lett.* **29**, 702 (1993).
70. T. Morioka and co-workers, *Electron. Lett.* **30**, 591 (1994).
71. A. D. Ellis and D. M. Spirit, *Electron. Lett.* **29**, 2115 (1994).
72. J. P. Hermann and J. Ducuing, *J. Appl. Phys.* **45**, 1500 (1974).
73. S. R. Friberg and P. W. Smith, *IEEE J. Quant. Elec.* **QE23**, 2089 (1987).
74. G. I. Stegeman and R. H. Stolen, *J. Opt. Soc. Am. B* **6**, 652 (1989).
75. X. F. Cao and co-workers, *J. Appl. Phys.* **65**, 5012 (1989).
76. A. N. Bain and co-workers, *Spectros. Int. J.* **8**, 71 (1990).
77. U. P. Wild and co-workers, *Appl. Opt.* **29**, 4329 (1990).
78. E. Zojer and co-workers, *J. Chem. Phys.* **80**, 3646 (2002).
79. W. Zhou and co-workers, *Science* **296**, 1106 (2002).

LARRY R. DALTON
DENISE H. BALE
University of Washington

Table 1. Comparison of Electrooptic Modulator Performance Parameters of NLO Materials^a

Parameter	LiNbO ₃	NLO polymer	GaAs
r_{eff} , pm/V	30	130	1.5
$n^3(r_{\text{eff}})^b$	330	584	64
ε	30	3	11
$n^3(r_{\text{eff}})/\varepsilon^b$	10	195	6
length · bandwidth product, GHz · cm	7	>100	10
$V_{\pi}L$, V · cm	5	2	0.3
optical loss, dB/cm	0.2	0.2–1.0	2

^a At optical wavelength of 1.3 μ .
^b Values given are figures of merit.

Table 2. NLO Chromophores and Corresponding $\mu\beta$ Values^a

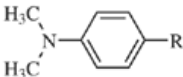
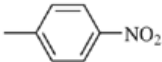

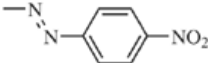
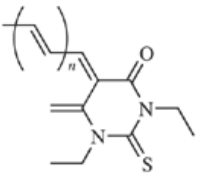
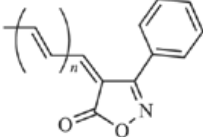
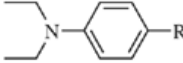
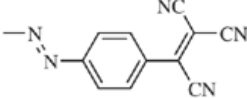
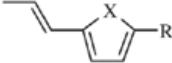
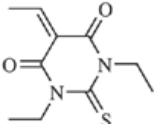
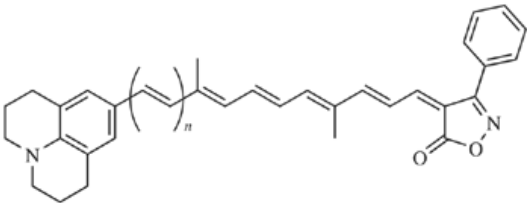
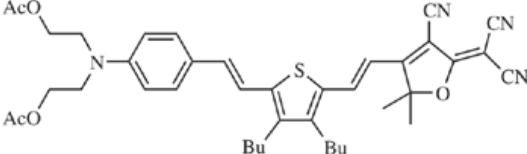
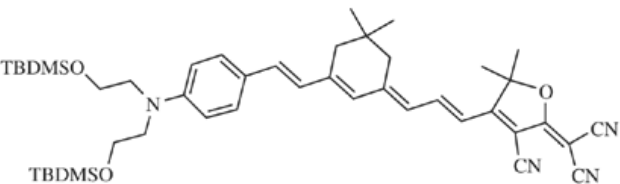
Chromophore base	R	Nonlinearity, $\mu\beta$, esu $\times 10^{-48}$
	NO ₂	140 ^{b,c}
		275 ^d
		580 ^e , 482 ^f ($n = 1$) 813 ^f ($n = 2$) 1074 ^f ($n = 3$) 1700 ^f ($n = 4$)
		800 ^{g,h}
		370 ^f ($n = 0$) 1457 ^f ($n = 1$) 3945 ^f ($n = 2$) 9831 ($n = 3$)
		312 ^f ($n = 0$) 1202 ^f ($n = 1$) 3156 ^f ($n = 2$) 8171 ^f ($n = 3$)
		4100 ^{g,h}
		560 ^d , (X = O, R' = NO ₂) 700 ^d (X = S, R' = NO ₂) 2400 ⁱ
		

Table 2. NLO Chromophores and Corresponding $\mu\beta$ Values^a

Chromophore base	R	Nonlinearity, $\mu\beta$, esu $\times 10^{-48}$
		28,500 ^f
		18,000 ^j
		>30,000 ^k

^aMeasured at 1.907 μm unless otherwise indicated. The parameter μ is the dipole moment and β is the molecular first hyperpolarizability defined in equation 1.

^bMeasured at 1.3 μm .

^cRef. 16.

^dRef. 17.

^eRef. 18.

^fRef. 19.

^gMeasured at 1.58 μm .

^hRef. 20.

ⁱRef. 21.

^jRef. 7.

^kRef. 22.

Table 3. **Second Harmonic Generation Coefficients of Inorganic Materials**

Material	Second harmonic generation coefficients, pm/V	Transparency window, nm
lithium niobate	$d_{15} = 6.3$ and $d_{22} = 3.3$	400–2,500
potassium dihydrogen phosphate	$d_{36} = d_{14} = d_{25} = 0.5$	200–1,500
ammonium dihydrogen phosphate	$d_{36} = d_{14} = d_{25} = 0.6$	200–1,200
potassium titanyl phosphate	$d_{33} = 15, d_{13} = 7, d_{32} = 5, d_{24} = 8, d_{15} = 7$	350–4,500
lithium formate monohydrate	$d_{31} = d_{15} = 0.107$ and $d_{32} = d_{24} = 1.25$	230–1,200
urea	$d_{36} = d_{14} = d_{25} = 1.42$	200–1,430
gallium arsenide	$d_{36} = d_{14} = d_{25} = 90$	900–17,000

Table 4. **Comparison of Kerr Effect Materials**

Material	Figure of merit							
	$n_2, \text{m}^2/\text{W}$	τ, s	Δn	α, cm^{-1}	W^a	T^b	$W', \text{m}^3/\text{W}$	$W'' \text{m}^3/(\text{W}\cdot\text{s})$
GaAlAs	10^{-12}	10^{-8}	2×10^{-3}	30	>1	>3	3×10^{-15}	3×10^{-7}
doped CdS glass	10^{-14}	10^{-11}	5×10^{-5}	3	>0.3		3×10^{-17}	3×10^{-6}
silica glass	10^{-20}	10^{-14}	$>10^{-6}$	10^{-5}	$>10^3$	<1	$>10^{-17}$	$>10^{-3}$
polydi-acetylene (PTS) crystal	10^{-16}	10^{-14}	$>10^{-3}$	<0.8	>10	<0.1	$>10^{-17}$	$>10^{-3}$
diaminonitro-stilbene polymer (DANS)	10^{-17}			<0.2	>5	>0.2	5×10^{-16}	

^aSee equation 18.^bSee equation 19.

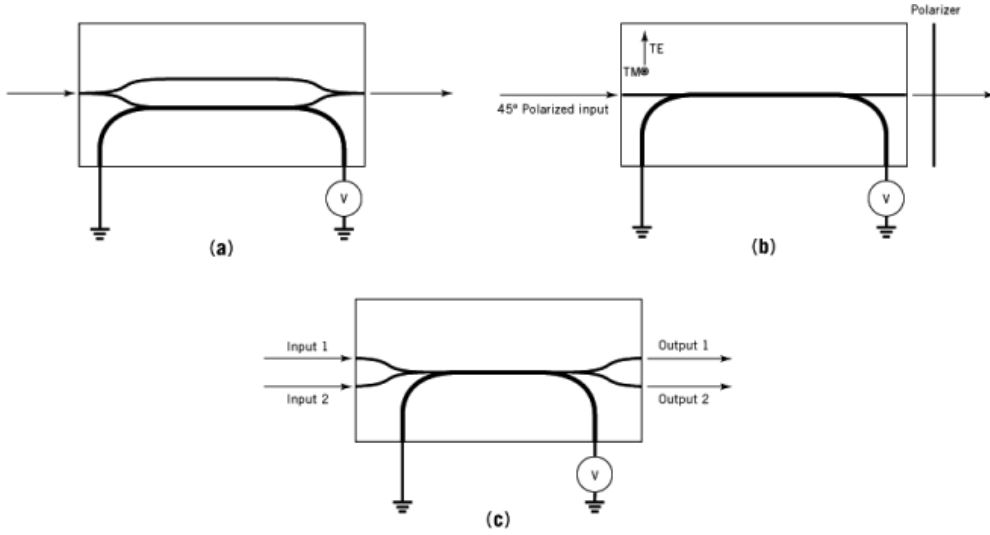


Fig. 1. Representative device configurations exploiting electrooptic second-order nonlinear optical materials are shown. Schematic representations are given for (a) a Mach-Zehnder interferometer, (b) a birefringent modulator, and (c) a directional coupler. In (b), the optical input to the birefringent modulator is polarized at 45° and excites both transverse electric (TE) and transverse magnetic (TM) modes. The applied voltage modulates the output polarization. Intensity modulation is achieved using polarizing components at the output.